Electron-Ion Recombination in a Sonic Orifice Flow

RICHARD C. JENKINS*
Grumman Aerospace Corporation, Bethpage, N. Y.

A comparison is made of measured and predicted axial variations of flow properties in a freely expanding plasma. Surveys of ion density and electron temperature were obtained in an arc-heated argon flow produced by expansion from a 0.635-cm-diam sonic orifice. Measurements were taken from current-voltage characteristics produced by uncooled electrostatic probes that were swept rapidly through the high temperature freejet. The flowfield calculations were based on an approximate analysis developed by Talbot, Chou, and Robben. Application of their analysis required modification to account for thermal nonequilibrium at the orifice. As a further modification, we have adopted a specific total density distribution which was empirically deduced.

1. Introduction

THIS paper describes an investigation of the effects of electron-ion recombination on the flow properties in a steady-state expansion of a partially ionized monatomic gas from a sonic orifice. The purpose of this work was to evaluate an approximate method of determining the flow properties in the test section of an arc-heated wind tunnel. We sought to develop a method that required a minimum of test section measurements. Our primary effort was directed toward approximate prediction of the level and variation of electron temperature in an expanding plasma. In flows with high ionization fraction, the speed of sound and Mach number are strongly dependent on electron temperature, particularly under conditions of thermal nonequilibrium. Also, the electron temperature must be known so as to deduce ion density from a measurement of probe ion saturation current. An accurate probe measurement of electron temperature is often difficult to obtain since one must record probe current at many different voltage levels. When the flowfield is turbulent or slightly unsteady (a condition often encountered in arc-heated flows or in short duration flows such as a shock tunnel), a reasonably accurate method of estimating local electron temperature may be more convenient than a direct measurement.

The variation of flow properties during a rapid expansion of a partially ionized gas is strongly influenced by electron-ion recombination. Under conditions encountered in many laboratory plasmas, this recombination is governed by a three-body collisional-radiative process in which the third body is an electron that carries off part of the recombination energy.[1-3] The recombination process provides energy that can elevate the electron temperature well above the heavy-particle temperature during the expansion. This type of recombination mechanism would account for the high levels of electron temperature that are often observed in rapidly expanded arc-heated flows.

An approximate analysis of electron-ion recombination effects in a Laval nozzle was presented by Talbot, Chou, and Robben,[4] and later extended by Chou and Talbot for the special case of a sonic orifice expansion.[5] Their method of analysis is approximate in that it yields only the upper and lower bounds to the actual flow properties, assuming for these bounds that the gas is either optically thick or optically thin. In their analysis, they used the reaction rate coefficients calculated by Bates et al.[1,2] for hydrogen, assuming that these rate coefficients could be applied to any singly ionized monatomic gas for an approximate analysis. The data presented by Robben, Kunkel and Talbot[3] provided some justification for this assumption. Further discussion of this assumption is presented in Ref. 4, which also presents a method of adapting the Bates' hydrogen radiation coefficients for use with argon.

For a partial evaluation of this type of analysis, we undertook a series of measurements in an arc-heated sonic orifice flowfield. The expansion region upstream of the normal shock in this type of freejet has been studied in detail at low temperature by a number of investigators (e.g., Refs. 6 and 7), and our previous investigation[8] of this type of plasma expansion suggested that the axial density distribution was predictable. Our measurements showed, however, that the level and variation of other flow properties could not be similarly predicted.

The preliminary data presented in Ref. 8 showed qualitative agreement with the theoretical results presented in Ref. 5. Vast differences in flow conditions, however, prevented a quantitative comparison. Our ion density levels were almost two orders of magnitude higher than Chou and Talbot[5] had assumed. In addition, a more fundamental difference ruled out a direct comparison. Their step-by-step calculations started from the orifice, at which point the flow was assumed to be in thermal equilibrium. As we show in a later section, the level of our ion density measurements proved conclusively that at the orifice our flow was not in thermal equilibrium. The electron temperature was significantly higher than the heavy-particle temperature.

For the present work, we modified Talbot's analysis to provide for nonequilibrium conditions at the orifice. We started our calculations at the orifice by taking into account differences in electron and ion temperature at this point. Evaluation of starting conditions for the calculations required measurement of bulk flow properties at the orifice and one flowfield measurement of ion density. The upper and lower limits on some orifice properties were established by iterating the flowfield calculations to match the calculated and measured ion density at one point in the expanded flow. We needed this one flowfield measurement to start our calculations because the nonequilibrium flow properties at the orifice could not be completely specified by bulk flow measurements alone.

The Langmuir probes used for this work were slender tungsten wire cylinders protruding from a glass sheath, a design used extensively at the University of Toronto[9,10] for free-molecular probe measurements. We used their data analysis procedures but adopted different data acquisition techniques for use with transient probes. These measurement techniques made it possible for us to obtain data at higher temperatures and higher ion density levels than those

Received September 28, 1970; revision received January 13, 1971. The author appreciates the help provided by H. Hopkins and T. Luzzi in a number of discussions of probe theory and data analysis.

* Research Engineer, Fluid Dynamics Section, Research Department. Member AIAA.

presented by most other investigators who have used this type of probe.

2. Flowfield Analysis

Since our objective is a comparison of our data with a modification of a theoretical analysis developed by other investigators, we will present only those equations necessary for our calculations and omit derivations already presented elsewhere. We adopt the notation used by Talbot, Chou, and Robben[4] for their continuum flow analysis of Laval nozzle flows and apply this analysis to a sonic orifice flowfield. The *CGS* unit system is used except where noted.

2.1 Basic Equations

The gas is assumed to be monatomic, only singly ionized, and everywhere electrically neutral ($n_e = n_i$). Further, we assume that the ion and neutral temperatures are equal throughout the flow, and that $m_i = m_a$. Assuming that the three species present individually obey the perfect gas law, the sum of the partial pressures yields

$$p = nk(fT_e + T) \tag{1}$$

where f is the ionization fraction, T is the heavy particle temperature, and $n = n_i + n_a$. Then, the local speed of sound is given by

$$a = [(5k/3m_a)(fT_e + T)]^{1/2} \tag{2}$$

We assume that no net current flows through the plasma. In combination with the requirement for local electrical neutrality, this implies that the velocity of all species is everywhere equal. Then, we can define a plasma Mach number as

$$M = u/a \tag{3}$$

The enthalpy per unit mass is given by

$$i = (5/2)(k/m_a)(fT_e + T) + (\chi/m_a)f \tag{4}$$

where χ is the ionization energy per atom.

2.2 Axial Density Distribution

In a low temperature expansion from a sonic orifice, the local Mach number along the centerline can be predicted from an expression developed by Ashkenas and Sherman.[11] For an isentropic expansion of a monatomic gas one can then find the centerline density distribution using the relation

$$n/n^* = 1.5396(1 + M_c^2/3)^{-3/2} \tag{5}$$

where n^* is the density at the orifice and M_c is the predicted cold flow Mach number.

In an earlier experimental investigation[8] of a plasma expansion from a sonic orifice, we found that measurements of ion density taken along the centerline upstream of the normal shock could be correlated with the low temperature density distribution. When Eq. (5) was normalized to agree with the measured ion density at one point in an axial survey, the remaining measurements followed this distribution. Thus the measured ion density distribution agreed with the predicted total density distribution, implying that the flow far from the orifice was chemically frozen.

Subsequent surveys carried out closer to the orifice revealed that the ion density decayed more rapidly than predicted by Eq. (5). The discrepancy between data and theory increased as surveys were carried out closer to the orifice. These observations suggested that the total density distribution in our plasma expansion was the same as that predicted for a corresponding low-temperature argon expansion, and that the discrepancy between ion density measurements and frozen flow theory could be attributed to electron ion recombination.

In this investigation, we have based our flowfield calculations on the simplifying assumption that the total density distribution in our freejet is identical to that predicted by Eq. (5) for a low-temperature argon flow from the same diameter orifice. This distribution is valid only in the region downstream of $x/D = 1$, where x is the axial distance from an orifice of diameter D. It is invalid in the neighborhood of the orifice. The density distribution close to the orifice is critically dependent on its geometry, and in fact, no exact flowfield solution exists that can describe the density distribution in the neighborhood of an orifice of arbitrary shape. We have, therefore, chosen to describe the density distribution in the region $0 < x/D < 1$ with an exponential decay. This distribution is denoted by the subscript e. We find

$$(n/n^*)_e = e^{-1.50389X/D} \tag{6}$$

The constant matches this distribution to Eq. (5) at $x/D = 1$, where the slopes of the two distributions are approximately equal.

Thus, we have chosen to deviate from Talbot's assumption[5] that $nux^2 = \text{const}$, and adopt instead a specified density distribution. This approach greatly simplifies the calculations since the actual density at any point in the expanding plasma can now be deduced from an estimate of density at the orifice. Furthermore, we can obtain, by differentiating the equations for (n/n^*), an analytic expression for dn/dx at any point.

2.3 Equations of Flow

Talbot and his associates found the following expression for the local electron temperature gradient:

$$\frac{dT_e}{dx} = \frac{2}{3}\frac{T_e}{n}\frac{dn}{dx} - \left[\left(T_e + \frac{2}{3}\frac{\chi_A}{k}\right)\Big/ f\right]\frac{df}{dx} - \frac{2R_A}{3n_iuk} - \frac{n_im_a}{u}(T_e - T)\left[D_1T_e^{-3/2}\ln\left(\frac{D_2T_e^3}{n_im_a}\right) + \frac{(1-f)}{f}D_3\right] \tag{7}$$

where the subscript A denotes properties for argon.

An expression of this general form appeared earlier in a paper by Bray,[12] who attributed its development to Wilson.[13] It is found from an energy conservation equation for free electrons. The particular form of the preceding expression, however, results from assumption of specific mechanisms of energy transfer between species and other assumptions that are described in detail in Refs. 4 and 5, to which the reader is referred for values of the constants D_1, D_2, and D_3. The numerical analysis makes use of this expression for the optically thin calculation as presented—for the optically thick calculation, $R_A = 0$.

The expression for df/dx is given by

$$df/dx = (-n_i/u)[(\alpha + S)f - S] \tag{8}$$

which Talbot developed from Bate's work.

The rate coefficients α, S, and R_A are functions of n_i and T_e. We evaluated these coefficients using the expressions presented by Talbot et al. in Ref. 4, where α, S, and R_A are found from power series approximations to Bates' tabulated theoretical rate coefficients for hydrogen.[1,2,14]

Consideration of the conservation equations for the ion and neutral species in a plasma yields the following expression for the local heavy-particle temperature gradient:

$$\frac{dT}{dx} = \frac{2T}{3n}\frac{dn}{dx} + \frac{n_im_af}{u}(T_e - T)\left[D_1T_e^{-3/2}\ln\left(\frac{D_2T_e^3}{n_im_a}\right) + \frac{(1-f)}{f}D_3\right] \tag{9}$$

where the constants D_1, D_2, and D_3 are the same as in Eq. (7).

The change in velocity between two points is found from consideration of the change in total enthalpy for both an optically thick and an optically thin gas. For an optically

thick gas, we assume no radial or axial heat transfer by conduction; thus, the expansion of an optically thick plasma can be considered an adiabatic process. Using Eq. (4), we find the following expression for total enthalpy per unit mass:

$$h = (5k/2m_a)(fT_e + T) + (\chi_A/m_a)f + u^2/2 \quad (10)$$

This relation can be evaluated to obtain h^* at the orifice, and then solved for velocity at downstream points.

For an optically thin gas, Talbot's analysis provided for radiation but for no absorption by adjacent fluid elements. The energy radiated is completely lost from the flow. If we again assume no conductive heat transfer, the optically thin flow is nonadiabatic only because of radiation losses; h is not constant, but its variation can be determined from consideration of radiative energy losses. Then, for our optically thin calculations, it was also possible to use Eq. (10) to compute the local total enthalpy. Starting from the orifice where the velocity was known, it was computed at downstream points by keeping in the calculation a running account of enthalpy loss due to radiation.

Once the flow properties are completely known at one point, Eqs. (7–10), together with the computed local values of n and dn/dx, can be used to calculate flow properties at downstream points. We used two separate calculations, one for an optically thick gas, and one for an optically thin gas.

2.4 Evaluation of Flow Properties at the Orifice

To start the calculations, we had to know all plasma properties at the orifice. Our measurements revealed that at the orifice the flow was in a state of thermal nonequilibrium. The assumption of thermal equilibrium yielded inconsistent results. Our probe measurements of ion density showed that at a point 0.75 cm downstream of the orifice, n_i was falling quite rapidly and yet was an order of magnitude higher than predicted at the orifice under thermal equilibrium conditions. In addition, at this point in the flow, we measured a value of T_e that was about the same as the deduced value of $(fT_e + T)^*$, and our data showed that T_e also was falling rapidly. From these observations, we concluded that $T_e^* > T^*$.

Thermal nonequilibrium is frequently encountered in gases heated by an arc discharge. Under such conditions, it is often found that the ionization level is determined by the electron temperature. If the electrons in higher energy states are in equilibrium with free electrons, one can compute the ionization fraction from the Saha equation using the electron temperature. An argument supporting application of this relation under thermal nonequilibrium conditions was given by Kerrebrock.[15]

We have assumed, therefore, that at the orifice the pressure, electron temperature, and ionization fraction are related by the expression

$$f^* = \left[1 + \frac{2.51 \times 10^5\, p^*}{(T_e^*)^{5/2}}\, e^{1.821 \times 10^5/T_e^*}\right]^{-1/2} \quad (11)$$

which was presented for argon in this form in Ref. 16. The value of p^* is given in atmospheres.

Pressure measurements were made with a small tap located within the orifice. Let p_h^* represent the orifice pressure measured in the high temperature flow, and let p_c^* represent the pressure measured with the same gas flow rate but with the arc off. Applying the continuity equation,

$$n_c^* u_c^* A_{ch}^* = n_h^* u_h^*$$

where A_{ch}^* represents the ratio of effective orifice areas under cold flow and hot flow conditions. Using Eqs. (1) and (2) for the hot flow and the corresponding ideal gas relations for the cold flow, we find the number density at the orifice is given by

$$n_h^* = n_c^* A_{ch}^* [p_c^*/p_h^*] \quad (12)$$

Similarly, we find the following expression for plasma temperature at the orifice:

$$(fT_e + T)^* = (T_c^*/A_{ch}^*)(p_h^*/p_c^*)^2 \quad (13)$$

The preceding expressions provide mean values for these flow properties at the orifice. These equations provided starting conditions for calculations of flow properties along the centerline for comparison with our measurements. Since radial gradients in flow properties undoubtedly exist, the actual centerline values of $(fT_e + T)^*$ should be somewhat higher, and n^* somewhat lower, than these equations predict. We have chosen a value of $A_{ch}^* = 1$ to provide at least some compensation for radial gradients. Because of the lower Reynolds in the hot flow, one would expect to encounter values of A_{ch}^* greater than 1.

To determine the individual values of f^*, T_e^*, and T^*, we used an iterative procedure based on the condition that calculated and measured ion density must agree at $x/D = 2$. In the calculation for an optically thick gas, different initial combinations of f^*, T_e^*, and T^* were chosen [consistent with Eqs. (11) and (13)] until the predicted and measured ion densities agreed at $x/D = 2$. This procedure yielded the flow conditions that would have had to exist at the orifice if the gas were optically thick. A similar iteration of the optically thin calculation yielded the starting conditions for the optically thin limiting assumption. Although this iterative procedure yielded sufficient information to begin either calculation, it could not provide actual values for f^*, T_e^*, and T^*, only the upper and lower bounds. The values found in this manner were used as the initial conditions for the integration of Eqs. (7–9).

Because our calculations utilized a specified density distribution, the program was simple enough to be run on a time-sharing computer. A Runge-Kutta technique was used to integrate Eqs. (7–9) from the orifice to a point where the effects of the presence of the normal shock caused deviation of the data from an undisturbed orifice expansion.

3. Experimental Measurements

The experiments were carried out in the Grumman Research Department arc tunnel. The flowfield was a freejet of argon from a 0.635-cm-diam port that was expanded to approximately 5 cm in outer diameter. The gas was arc-heated shortly upstream of the orifice with a wall-stabilized arc chamber that required no gas vortex. Figure 1 shows a sketch of the flowfield and orifice geometry. The orifice exhausted into a water-cooled test tank that was pumped continuously by a two-stage mechanical pump assembly that maintained the tank pressure at less than 1 torr for these tests. The nozzle pressure ratio was nominally 200.

3.1 Probe Measurement Technique

The Langmuir probe was a glass-encased 0.025-mm-diam tungsten wire with 2.08-mm length exposed for measurement. The insulator diameter in the vicinity of the probe tip was 0.25 mm. The probes were mounted on an axial traverse system that was supported by a rotating shaft that passed through the front wall of the vacuum tank. Shaft rotation provided lateral probe motion through the freejet. Axial

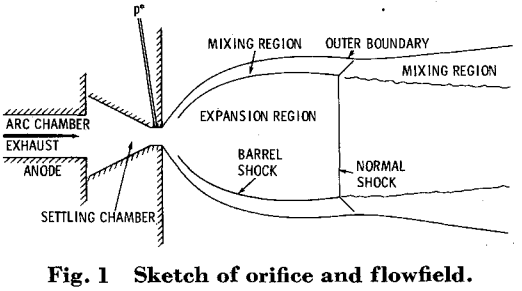

Fig. 1 Sketch of orifice and flowfield.

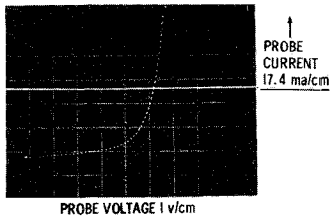

Fig. 2 Typical Langmuir probe signal.

motion was provided by an externally controlled screw drive on the probe support. Rapid probe movement through the freejet was required to avoid overheating the probe.

A 700-*Hz* sawtooth voltage was applied to the probe electrode (biased against the arc anode) and the probe signal was displayed as current vs voltage on an oscilloscope. As the probe was swept through the flow a series of probe characteristics could be observed that formed a closely packed family of curves. To display only one of these probe characteristics we used a trigger circuit (described in Ref. 8) to enhance oscilloscope trace light intensity when the probe was on the flow centerline. A typical probe signal is shown in Fig. 2.

The methods used to obtain ion density from this type of probe signal have been described in Ref. 8. The ion density was found from the equation

$$I_i/A = I_L e n_i (kT_e/2\pi m_i)^{1/2} \tag{14}$$

where I_i represents the ion current measured in the saturation region at a prescribed voltage relative to the probe floating potential V_f. I_L is a function of probe potential V, of T_i/T_e, and of the ratio of probe radius to Debye length. I_L has been evaluated from theoretical calculations of the entire probe characteristic for a cylindrical probe in an argon plasma and was presented in graphic form by Sonin in Ref. 9.

The electron temperature was found from the probe characteristic by using the relation

$$d(\ln I_e)/dV = e/kT_e \tag{15}$$

where I_e is the current flow due to electrons arriving at the probe. I_e was measured on an oscilloscope trace at small voltage increments and plotted vs voltage on semilog paper to determine T_e.

The probe electrodes were cleaned at approximately 1 torr in an argon atmosphere by a high voltage discharge from a Tesla coil. It was found necessary to reclean the probes each time they were exposed to atmospheric conditions. When the electrodes were adequately cleaned, a semilog plot of probe electron current vs voltage was linear over at least two orders of magnitude.

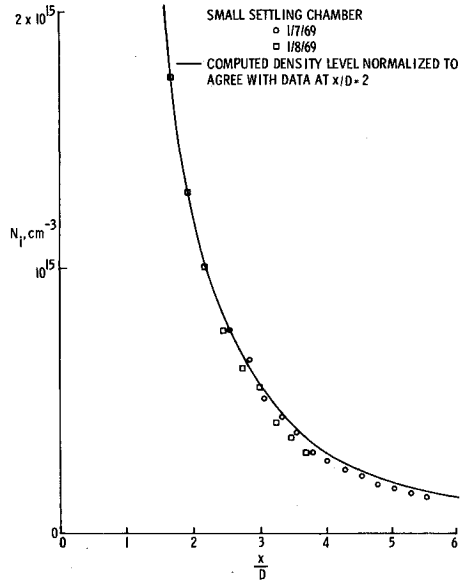

Fig. 3 Ion density survey compared to frozen flow expansion.

Table 1 Approximate mean free paths

Mean free paths involving neutrals	Small settling chamber $x/D = 2$	Small settling chamber $x/D = 5$	Large settling chamber $x/D = 2$	Large settling chamber $x/D = 5$
λ_{aa}	0.26 *mm*	1.4 *mm*	0.18 *mm*	0.67 *mm*
λ_{ia}	0.073	0.37	0.048	0.19
λ_{at}	0.33	2.1	3.7	18
λ_{ea}	58	300	27	480
Charged particle mean free paths				
λ_{ee}	0.01	0.02	0.02	0.2
λ_{it}	0.003	0.003	0.004	0.005

3.2 Sources of Probe Measurement Error

To obtain freestream measurements, the probe should operate under free-molecular conditions to minimize disturbances in the incident plasma. If the axis of the probe electrode is aligned with the flow, the diameter of the electrode (and also adjacent sections of insulating glass) should be much smaller than any of the local mean free paths. Consideration of Table 1 shows that the probe electrode diameter d was small compared to mean free paths involving neutrals, but was operating in a transition flow with respect to charged particles. This situation cannot be avoided in probe investigations of high ion density plasmas, particularly at relatively low plasma temperatures.

Other investigators[9,10] have shown that small values of λ_{ii}/d do not provide a measurable source of error in Langmuir probe electron temperature measurements, but that the ion density measurements may not yield actual freestream values. Sonin[9] conducted a detailed study of probe behavior at ion densities in the range of 10^{13} cm^{-3}, and found satisfactory probe response with λ_{ii}/d in the range of 0.03 to 0.5. Although our ion density levels were an order of magnitude higher than Sonin's, our ion temperatures were also an order of magnitude higher, and our ratio of λ_{ii}/d was in the same range. Based on this comparison, we believe that this source of probe error may not have been significant.

An additional source of probe error involves the effective probe electrode area. Physical area was measured accurately by microscope. Sonin found that the presence of electrode end effects was negligible for a probe length-to-diameter ratio greater than 100. In our work, we chose a ratio of 80. In view of the relatively small sheath thickness, we believe no significant error was associated with probe length except possibly the averaging of our measurements over a finite probe length in regions of high ion density gradients.

A further source of error could be the presence of contaminants in the flow. We used a commercial grade of argon rather than ultra-high-purity argon. Thus nitrogen, oxygen, and water vapor were present in the flow to some extent. In addition, there was an undetermined level of tungsten and copper contamination present in the flow from the arc electrodes. Because of the approach chosen for electron temperature data reduction, we are convinced that the probe data are not in error because of such contaminants. However, it is possible that the entire flowfield chemistry could be affected by the presence of trace contaminants. Most likely, such effects would be less noticeable at high ionization frac-

Table 2 Operating conditions

Settling chamber	Arc current	Arc voltage	Argon flow rate	p^*	n^*	$(fT_e + T)^*$
Small	510 amp	16 v	0.35 g/sec	86.5 torr	1.114×10^{17}	7500°K
Large	550 amp	16 v	0.47 g/sec	79.0 torr	1.996×10^{17}	3820°K

tion. It is difficult to assess the extent and the effects of such trace contamination, other than to recall Talbot's basic assumption that Bates' reaction rate constants should be applicable to any singly ionized monatomic gas. At any rate, our intent here was to obtain partial evaluation of Talbot's analysis using conditions often encountered with a practical laboratory plasma.

4. Comparison of Data and Theory

Data are presented for two different flowfields that were obtained using different settling chamber volumes but the same 0.635-cm-diam orifice. The smaller settling chamber is shown in Fig. 1. The test flow conditions are shown in Table 2.

Figure 3 presents the ion density distribution obtained using the small settling chamber compared with the total density distribution predicted by Eq. (5). The theoretical curve was normalized to match the data at $x/D = 2$. If the predicted number density distribution was valid, one would expect the data to agree with the theory only if the chemical composition remained frozen beyond $x/D = 2$. If the ionization fraction decreased beyond this point because of electron-ion recombination, one would expect the data to fall below the predicted level at downstream points.

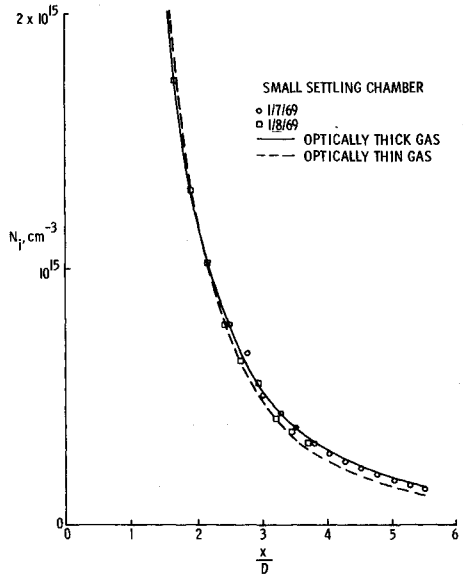

Fig. 4a Ion density survey compared to expansion with recombination (small settling chamber).

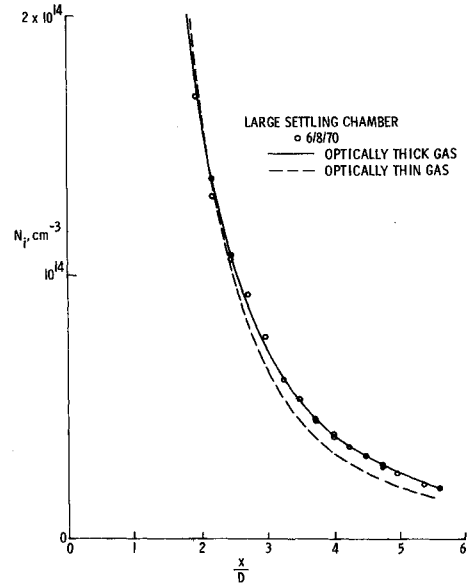

Fig. 4b Ion density survey compared to expansion with recombination (large settling chamber).

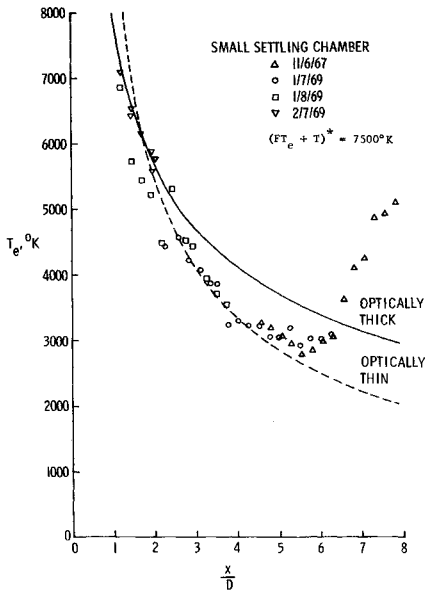

Fig. 5a Electron temperature survey compared to predicted upper and lower bounds (small settling chamber).

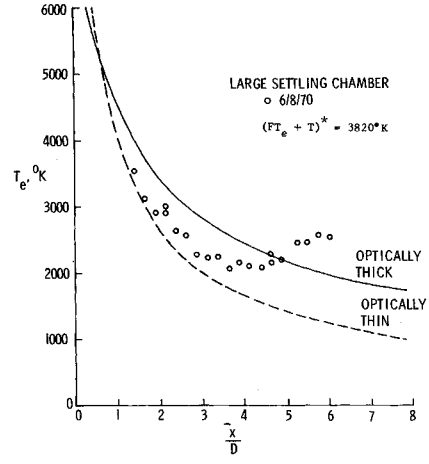

Fig. 5b Electron temperature survey compared to predicted upper and lower bounds (large settling chamber).

Figures 4a and 4b provide a comparison between our ion density data and the upper and lower limits predicted by the flowfield calculations described in Sec. 2. The curves for the optically thick and optically thin distributions cross at $x/D = 2$ because we have used the ion density level measured at this point to establish starting conditions for our calculations. Since the data shown in Figs. 3 and 4a are the same, a comparison (theory vs theory) of these two figures indicates the degree of recombination predicted by the optically thick and optically thin limiting assumptions. Only a comparison (data vs theory) of the axial density variation is meaningful since the measured ion density level was used to start the calculations. This latter comparison is somewhat limited in value because of the small amount of recombination that was observed within the region of flow that was surveyed. However, our calculations show a level of recombination that approximately accounts for the discrepancy between data and theory in Fig. 3.

We were mainly interested in the ability of this type of analysis to predict approximately local electron temperature. Figures 5a and 5b show that the theory provided a good approximation for the level and variation of electron tempera-

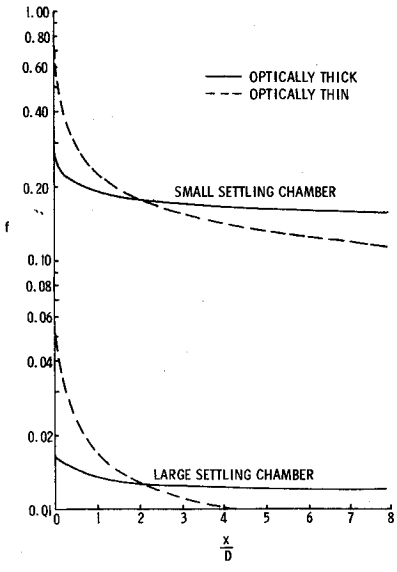

Fig. 6 Computed variation of ionization fraction.

ture along the centerline in the region of plasma expansion that was free of shock wave effects. The data lie closer to the optically thin predictions. The greater degree of scatter relative to the ion density data reflects inaccuracies inherent in replotting an oscilloscope trace.

Our electron temperature measurements showed a deviation from the predicted variation starting at about $x/D = 6$ in Fig. 5a and $x/D = 4$ in Fig. 5b. A similar deviation was noted in the corresponding ion density measurements but further downstream at approximately $x/D = 8$. The break in the ion density distribution indicates the onset of plasma compression associated with the normal shock. Figures 5a and 5b show that the electron temperature begins to increase well upstream of the normal shock. Christiansen[17] observed a similar rise in electron temperature upstream of a shock produced by a blunt body in an ionized flow of cesium-seeded argon. His investigation of the shock structure indicated that the electron temperature increased through the shock because of compression heating, and that energy transfer by electron thermal conduction brought about the electron temperature rise ahead of the compression region.

The flowfield calculations yielded reasonably close upper and lower limits on electron temperature. Within the undisturbed regions of plasma expansion, these upper and lower bounds were at most $\pm 15\%$ of the mean value (at high x/D) and were less than $\pm 10\%$ throughout most of the expansion. This difference between upper and lower bounds is of the same order as the scatter frequently encountered in probe measurements of electron temperature. The electron temperature is often of interest primarily for predicting local speed of sound or for converting saturation iron current measurements to ion density. In the latter case, $(T_e)^{1/2}$ is used, and in the former case, $(fT_e + T)^{1/2}$. For such applications, even a crude estimate of electron temperature will contribute little source of error.

Our flowfield calculations also provided upper and lower bounds for ionization fraction, heavy-particle temperature, velocity, speed of sound, and Mach number. The favorable comparison shown in Figs. 5a and 5b provides some justification for accepting the upper and lower limits predicted for these other variables. We found the upper and lower bounds on heavy particle temperature were quite close, being at most $\pm 5\%$ of the mean value. The bounds on flow velocity were similar, and on Mach number were somewhat greater, reaching $\pm 8\%$ at high x/D. The bounds on ionization fraction, presented in Fig. 6, were considerably wider because of vast differences in recombination rates under optically thick and optically thin conditions.

With regard to plasma conditions at the orifice, the upper and lower bounds were close enough to estimate, $T_e^* = 12{,}000°K$ for the small settling chamber, and $T_e^* = 9000°K$ for the large settling chamber. For the small settling chamber, we could not obtain a reasonable lower limit to heavy particle temperature at the orifice from the optically thin calculation—the value required to start the calculation was close to 0°K. The optically thick calculation provided $T^* = 4250°K$ as an upper bound. For the large settling chamber, we found $T^* = 3700°K$ for the upper limit and $T^* = 3320°K$ for the lower limit. Such estimates provide a rough measure of thermal nonequilibrium at the orifice. For the large settling chamber, we conclude that $2.4 < (T_e/T)^* < 2.9$, whereas for the small settling chamber, we can only state that $2.7 < (T_e/T)^*$.

Some of the calculations presented by Chou and Talbot[5] demonstrate that thermal nonequilibrium conditions should be expected to exist at the sonic point when a plasma is assumed to expand from equilibrium stagnation conditions. However, the degree of thermal nonequilibrium that we encountered at our orifice appears considerably greater than their calculations would predict. We believed that this type of analysis could not describe the orifice conditions that we observed. First, our settling chamber was too small to provide a stagnation region with equilibrium conditions upstream of the orifice, and second, one would expect to encounter thermal nonequilibrium shortly downstream of a high-intensity electric discharge.

5. Concluding Remarks

We found that the method of analysis developed by Talbot and his associates provided a description of our flowfield that was consistent with our measurements and relatively direct in application. Two modifications of their calculational techniques were undertaken to adapt his analysis to our particular experimental situation. These modifications made it possible to use a single ion density measurement, in combination with bulk plasma properties measured at the orifice, to calculate approximate upper and lower bounds on the flow properties throughout the undisturbed expansion region downstream of a sonic orifice. We found that this approach predicted with reasonable accuracy the level and variation of electron temperature in an expanding argon plasma.

Our assumption that the total density distribution is the same as in a low-temperature argon expansion from the same orifice was suggested by consideration of a number of axial surveys of ion density distribution. Reasonably good agreement between electron temperature measurements and predictions based on this density distribution further support this assumption. The exponential function we arbitrarily chose to represent the density distribution in the neighborhood of the orifice appears to be satisfactory for approximate prediction of the electron temperature variation downstream of the orifice.

Our results tend to verify Talbot's assumption that Bates' hydrogen reaction rate coefficients can be applied to an argon plasma expansion for an approximate analysis of electron-ion recombination effects. A more critical test of this assumption would be encountered in a Laval nozzle flow since the slower plasma expansion and more extensive region of influence of chemical reactions would make the final test section conditions more sensitive to the reaction rate expressions.

6. References

[1] Bates, D. R., Kingston, A. E., and McWhirter, R. W. P., "Recombination between Electrons and Atomic Ions. I. Optically Thin Plasmas," *Proceedings of the Royal Society*, Vol. A, 267, 1962, pp. 297–312.

[2] Bates, D. R., Kingston, A. E., and McWhirter, R. W. P., "Recombination between Electrons and Atomic Ions. II. Optically Thick Plasmas," *Proceedings of the Royal Society*, Vol. A, 270, 1962, pp. 155–167.

[3] Robben, F., Kunkel, W. B., and Talbot, L., "Spectroscopic Study of Electron Recombination with Monatomic Ions in a Helium Plasma," *Physical Review*, Vol. 132, No. 6, 1963, pp. 2363-2371.

[4] Talbot, L., Chou, Y. S., and Robben, F., "Expansion of a Partially-Ionized Gas Through a Supersonic Nozzle," Rept. AS-65-14, Aug. 1965, Univ. of California, Berkeley, Calif.

[5] Chou, Y. S. and Talbot, L., "Source-Flow Expansion of a Partially Ionized Gas into a Vacuum," *AIAA Journal*, Vol. 5, No. 12, Dec. 1967, pp. 2166-2172.

[6] Love, E. S., Grigsby, C. E., Lee, L. P., and Woodling, M. J., *Experimental and Theoretical Studies of Axisymmetric Free Jets*, TR R-6, 1959, NASA.

[7] Owen, P. L. and Thornhill, C. K., *The Flow in an Axially Symmetric Supersonic Jet from a Nearly Sonic Orifice into a Vacuum*, Rept. 30/48, 1948, Ministry of Supply, Armament Research Establishment, Great Britain.

[8] Jenkins, R. C., *Electrostatic Probe Measurements in a Partially Ionized Free Jet from a Sonic Orifice*, Rept. RE-333, July 1968, Grumman Research Dept., Grumman Aerospace Corp., Bethpage, N.Y.

[9] Sonin, A. A., "Free-Molecule Langmuir Probe and Its Use in Flowfield Studies," *AIAA Journal*, Vol. 4, No. 9, Sept. 1966, pp. 1588-1596.

[10] Graf, K. A., *The Determination of Spatially Non-Uniform Electron Density Distribution*, UTIAS Rept. 108, April 1965, Univ. of Toronto.

[11] Ashkenas, H. and Sherman, F. S., "The Structure and Utilization of Supersonic Free Jets in Low Density Wind Tunnels," *Rarefied Gas Dynamics*, Vol. II, edited by J. Laurmann, Academic Press, New York, 1963, Sec. 7,

[12] Bray, K. N. C., "Electron-Ion Recombination in Argon Flowing Through a Supersonic Nozzle," AGARDograph 68, 1963, pp. 67-87.

[13] Wilson, J. A., Ph. D. thesis, 1962, Univ. of Southhampton, England.

[14] Bates, D. R. and Kingston, A. E., "Properties of a Decaying Plasma," *Planetary and Space Science*, Vol. 1, No. 11, 1963, pp. 1-22.

[15] Kerrebrock, J. L., "Magnetohydrodynamic Generators with Nonequilibrium Ionization," *AIAA Journal*, Vol. 3, No. 4, April 1965, pp. 591-601.

[16] Norman, W., *One-Dimensional Magnetohydrodynamic Equations for a Non-Ideal Gas with Application to Singly Ionizing Argon*, AEDC-TR-65-185, Arnold Engineering Development Center, Arnold Air Force Station, Tenn, 1965.

[17] Christiansen, W. H., "Study of Shock Waves in a Nonequilibrium Plasma," *The Physics of Fluids*, Dec. 1967, pp. 2586-2595.

JULY 1971 AIAA JOURNAL VOL. 9, NO. 7

A Variable Phase Velocity Traveling Wave Pump

CHARLES W. HALDEMAN,* JOHN P. SULLIVAN,† AND EUGENE E. COVERT‡
Massachusetts Institute of Technology, Cambridge, Mass.

Results of analytical and experimental studies of an electrodeless, alternating-current plasma accelerator, the traveling wave pump, are presented. A coil assembly that produces a variable phase velocity and eliminates end effects is used. Data is presented indicating supersonic acceleration of argon plasma in qualitative agreement with the mathematical model.

Nomenclature

r,θ,z = circular cylindrical coordinates
A_θ = azimuthal component of vector potential
$\hat{a}_r,\hat{a}_\theta,\hat{a}_z$ = unit vectors
a = speed of sound
$\mathbf{B}$ = magnetic flux density
B_{eff} = effective amplitude of magnetic flux density; $0.5\text{-}(\mu NI)^2(kr_0)^2K_1^2(kr_0)[I_1^2(kr_0) - I_0(kr_0)I_2(kr_0)] = B_{\text{eff}}^2$
C = capacitance per unit length
$\mathbf{E}$ = electric field
G = Green's function
I = current per turn in exciting coil
$I_n(x)$ = modified Bessel function of the first kind of order n and argument (x)
$\mathbf{J}$ = current density
$J_n(x)$ = Bessel function of the first kind of order n and argument (x)
$\mathbf{K}$ = current sheet intensity
$K_n(x)$ = modified Bessel function of the second kind of order n and argument (x)
k = wave number
k_n = $\lambda n/R$
L = inductance per unit length, length
M = Mach Number
M_0 = initial Mach Number
N = number of turns per unit length on exciting coil
P = pressure
P_0 = isentropic stagnation pressure
R = radius of channel, resistance
T = temperature
t = time
u = velocity
$\bar{u}$ = time averaged component of velocity
u_0 = initial velocity
u' = unsteady component of velocity
V_p = phase velocity of magnetic wave $V_p = \omega/k(z)$
z = axial position (m)
γ = ratio of specific heats
λ_n = nth root of $J_0(x) = 0$
μ = magnetic permeability = $4\pi \times 10^{-7}$ h/m in free space
ξ = length parameter $\xi = \int(\sigma B_{eff}^2/\rho u)dz$
ρ = mass density
σ = electrical conductivity
ω = angular frequency

Received September 23, 1970; revision received March 23, 1971. This investigation was sponsored by the Aerospace Research Laboratories, Air Force Systems Command, U.S. Air Force, under Contract F33615-68-C-1380, and the Microwave Physics Laboratory, Air Force Cambridge Research Laboratories, Office of Aerospace Research, U.S. Air Force, under Contract F19628-69-C-0043.

* Associate Director, Aerophysics Laboratory. Member AIAA.

† Research Assistant, Department of Aeronautics and Astronautics.

‡ Professor. Associate Fellow AIAA.

Introduction

IN the classic rocket or wind-tunnel propulsion system, the enthalpy of the working fluid is converted to velocity (or Mach number) by an adiabatic expansion through a deLaval